Front. Struct. Civ. Eng. 2019, 13(4): 990–997
https://doi.org/10.1007/s11709-019-0532-8

RESEARCH ARTICLE

Bending performance of composite bridge deck with T-shaped ribs

Qingtian SU, Changyuan DAI, Xu JIANG*

Department of Bridge Engineering, Tongji University, Shanghai 200092, China
**Corresponding author. E-mail: jiangxu@tongji.edu.cn*

ABSTRACT This paper proposes a new type of steel-concrete composite deck, which is composed of orthotropic steel deck (OSD) with T-shaped ribs, concrete plate and studs connecting OSD and concrete plate. The OSD can act as framework for concrete plate and contribute to load bearing capacity at the same time, which could save construction time. Compared with conventional OSD system, this new type of composite bridge deck can also improve fatigue performance.

Considering that this type of composite deck is not yet applied in practical engineering and its mechanical performance is not revealed in previous literatures, two full-scale specimens were designed and manufactured in this research. The mechanical performance, particularly, bending capacity in positive and negative region was carefully tested and analyzed. The load-deflection curve, load-slip relation, strain distribution in concrete and steel were obtained. The test results showed that the plastic performance of this kind of composite bridge deck was satisfying and the bending capacity was high.

KEYWORDS bending performance, composite bridge deck, T-shaped steel ribs

1 Introduction

Bridge decks which is directly subjected to vehicle load are one of the most vulnerable component of a bridge [1]. The most common forms of bridge decks include steel bridge deck, concrete bridge deck, and steel-concrete composite bridge deck [2]. Concrete bridge decks are often applied in short-span bridges owing to its integrity and economy. However, the heavy self-weight of concrete restricts its application in long-span bridges [3]. Besides, due to the low tensile strength of concrete, cracking is inevitable when subjected to tensile stress [4]. Bi-directional mesh cracking, unidirectional cracking, breaking, and spalling are the main cracking forms of concrete bridge decks [5,6]. Steel bridge decks are most commonly applied in long-span bridges, while the high cost makes it diseconomy when applied in short-span bridges. Orthotropic steel deck (OSD) with trough ribs is the most popular form of steel bridge deck. However, fatigue cracks always initiated from the rib-to-deck plate weld because single-side welding is used to connect trough ribs and deck plates [7]. In addition, the rib-to-floorbeam connection, rib and deck splices and wearing surface of OSDs are also often subjected to fatigue cracks [8,9].

Due to various advantages of composite structures, steel-concrete composite decks appear in recent years [10]. It has been widely used for the infrastructure applications, such as composite beams and columns. For the profiled steel-concrete composite slab, a promising application is used as building floor slabs [11–14]. However, in the field of bridge engineering, the utilization of steel-concrete composite slabs is quite limited. In the research of Kim and Jeong [15–17], a steel-concrete composite deck slab system with profiled steel sheeting and perfobond rib shear connectors was investigated regarding to push-out tests, deck-to-girder connection tests, and full-scale tests. The research results concluded that the initial concrete cracking load and ultimate loading capacity of the proposed deck system is at least 230% and 220% greater than the corresponding values of a traditional RC deck slab, respectively, while the self-weight of proposed deck system was about 23% less than that of RC deck system.

Article history: Received May 30, 2017; Accepted Jan 8, 2018

The advantages of steel-composite bridge decks can be drawn as follows: First, the steel plate of the composite deck can act as the framework of concrete. Second, the concrete plate of composite deck can offer firm bond to the pavement, which in turn improve the pavement durability and reducing its maintaining cost. Third, composite deck can be prefabricated in the factory and thus the deck quality can be guaranteed easily and the construction time can be saved.

Hitherto, the main types of composite bridge decks include profiled steel sheet-concrete composite deck, plain steel plate-concrete composite deck, and so on [19]. These kinds of composite bridge decks are less than 200 mm in height, and shows poor flexure performance compared to that of OSDs. Thus, a new type of steel-concrete composite deck with T-shaped ribs is proposed in this paper, comprising of steel plain plate and concrete overlay. This new-type of composite bridge deck can improve bending capacity and flexural stiffness. It is worth to be mentioned that this new-type of composite bridge is not supposed to take the place of orthotropic steel decks for all type of bridges, but offers an alternative for the deck of the bridges. For example, in cable-stayed bridge, concrete deck can be used for the main-span less than 600 m, also steel deck can be used for the main-span larger than 400m, so composite deck can be used for the main-span between 300 to 800 m with acceptable self-weight and economic. So far orthotropic composite deck is not yet applied in the practical engineering and its mechanical performance are not yet revealed in previous studies. To test the mechanical performance of this kind of composite bridge deck, two specimens with different sections are designed and fabricated. The strain and displacement of the specimens under different load cases are tested and the mechanical behavior is investigated.

2 Experiment

2.1 Test specimens

Two steel-concrete composite deck specimens with T-shaped ribs (denoted as S-1 and S-2) were designed for quasi-static tests. In practical engineering, bridge decks are supported on floorbeams and the distance between floorbeams usually is 3 to 5 m [19]. Therefore, the specimens span length in the tests is selected to be 5m. To study the mechanical performance of this kind of composite bridge deck in positive and negative moment region, two two-span continuous composite bridge deck specimens each with a total length of 10.5 m (with 250 mm cantilever length at each outer side of the two side supports) is manufactured.

For specimen S-1, the cross section is shown in Figs. 1(a) and 1(b). The section depth is about 300 mm. The concrete overlay is 900 mm wide and 100 mm high, respectively. The longitudinal and transverse reinforcements are embedded in the concrete. The spacing and diameter of longitudinal rebars are 150 mm and 20 mm, respectively. While that of transverse rebar are 150 mm and 12 mm, respectively. The deck plate thickness of OSDs is 6 mm. The type of T-shaped ribs is TN200 × 200 hot rolled steel. Stud shear connectors used to connect steel plate and concrete overlay have a height of 80 mm and diameter of 13 mm. The transverse and longitudinal spacing of the stud connectors are 225 mm and 200 mm, respectively.

For specimen S-2, the concrete overlay is 1100 mm in width and 120 mm in height, respectively. The spacing and diameter of longitudinal rebars are 150 mm and 20 mm, respectively. That of transverse rebars are 150 mm and 12 mm, respectively. The deck plate thickness of OSDs is 6mm which is the same with S-1. While, the type of T-shaped ribs are TM170 × 250 hot rolled steel, the weight of which is almost the same with the T-shaped ribs applied in S-1. The dimension of studs is identical with S-1. However, the transverse and longitudinal spacing of the studs are 220 mm and 200 mm, respectively. The concrete cover thickness of the two specimens is 40 mm.

The self-weight of the two composite bridge deck specimens is about 5 kN/m^2, and that of the orthotropic bridge deck is about 3.5 kN/m^2 for the top plate with 16 mm thickness (both including asphalt pavement). The net self-weight of the composite decks is 42% larger than that of the orthotropic steel deck, but the total weight of main girder with composite deck is about 10% to 14% larger than that of main girder with composite deck taking account for the deck weight is about 30% to 40% of the main girder weight. Thus, the new type of composite decks

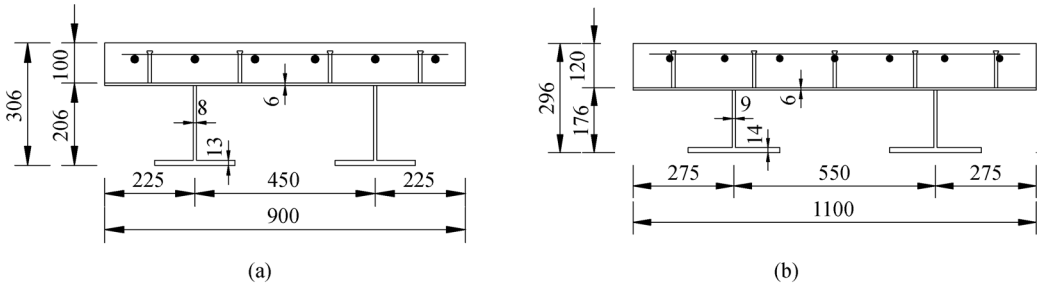

Fig. 1 Dimension of the specimens (unit: mm). (a) Cross section of S-1; (b) cross section of S-2

is not that applicable to super-long span bridges, but for middle-span and long-span bridges, the merits of higher fatigue strength and better pavement performance can make the efforts to extend the service life the bridge decks.

2.2 Test setup

To test the mechanical performance of this kind of composite bridge deck in positive and negative moment region, the two specimens (S-1 and S-2) were loaded at mid-span, as shown in Fig. 2. The mid-support was a fixed hinged support and the two side supports were movable hinged supports.

2.3 Measurement

To measure the stress distribution of the two specimens, strain gauges are employed. The strain gauges layout of specimen S-1 is shown in Fig. 3. Seven longitudinal strain gauges are mounted at the mid-span section (denoted as section A-A) and mid-support section (denoted as section B-B) respectively as shown in Fig. 3(a), to measure the longitudinal strain of the deck plate. Five longitudinal strain gauges are mounted on the top surface of the concrete plate at section B-B, as shown in Fig. 3(b). Four strain gauges are mounted on the reinforcement at the mid-support section, mid-span section and quarter-span section, respectively, as shown in Fig. 3(c). The arrangement of strain gauges of specimen S-2 is identical with that of S-1.

3 Test results and discussions

3.1 Material test

The material properties were tested. The real dimension, yield strength and tensile strength of steel are shown in Table 1 and the cubic compressive strength, tensile strength, and elasticity modulus of concrete are shown in Table 2.

3.2 Failure modes

At early loading stage, specimen S-1 behaved linearly with the increase of load. First crack appeared in concrete plate at section B-B, when the load increased to 30 kN. Thereafter, the width, depth, and number of cracks increased with the increase of load. When the load increased to 130 kN, the crack width and crack depth reached 0.2 mm and 35 mm, respectively. The bond between concrete slab and steel plate failed accompanied with loud noise when the load increased to 350 kN. At the same time, the depth of crack reached 58 mm. With the load continue to increase and reach 600 kN, the bottom flange of the T-shaped rib at section B-B yielded. Then followed the yielding of the bottom flange of the T-shaped rib at section A-A, strain and deformation of the specimen S-1 increased significantly. The concrete at section A-A crushed due to the large longitudinal compressive stress when the load increased to 810 kN (shown in Fig. 4). By this time, the specimen reached its ultimate state.

Specimen S-2 experience similar failure process with specimen S-1. First concrete crack appeared at section B-B when load increased to 40 kN. The crack width and maximum crack depth reached 0.2 mm and 29 mm when load increase to 140 kN. The yielding of bottom flange of T-shaped rib at section B-B and A-A appeared at the load level of 770 kN. At the ultimate stage when load increased to 950 kN, the concrete at section A-A crushed (shown in Fig. 5). The relative slip between the steel and concrete interface was found not notable in both specimens.

Until failure of the two specimens, local buckling of the rib wall was not observed.

3.3 Load-deflection relation

Based on the tested deflection of section A-A (averaged value of the two spans), load-deflection relation curve of the two specimens can be obtained.

As shown in Fig. 6, the load-deflection curve of the two specimens both exhibited elastic stage and plastic stage. When the applied load reach 585 kN and 737 kN for specimen S-1 and S-2, respectively, the specimens began to show nonlinear behavior. The ultimate load of the two specimens was 810 kN and 950 kN, respectively, as illustrated in section 3.2.

Since the width of the two specimens was different and to reasonably analyze and compare the load-deflection curves of the two specimens, the full-width load capacity was transformed to the load capacity per meter width by dividing the load value by the specimen width (0.9 for S-1 and 1.1 for S-2). The unit width load-deflection curves of

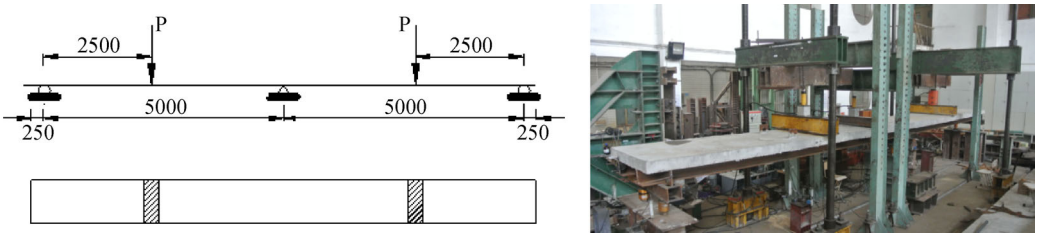

Fig. 2 Setup of the loading system

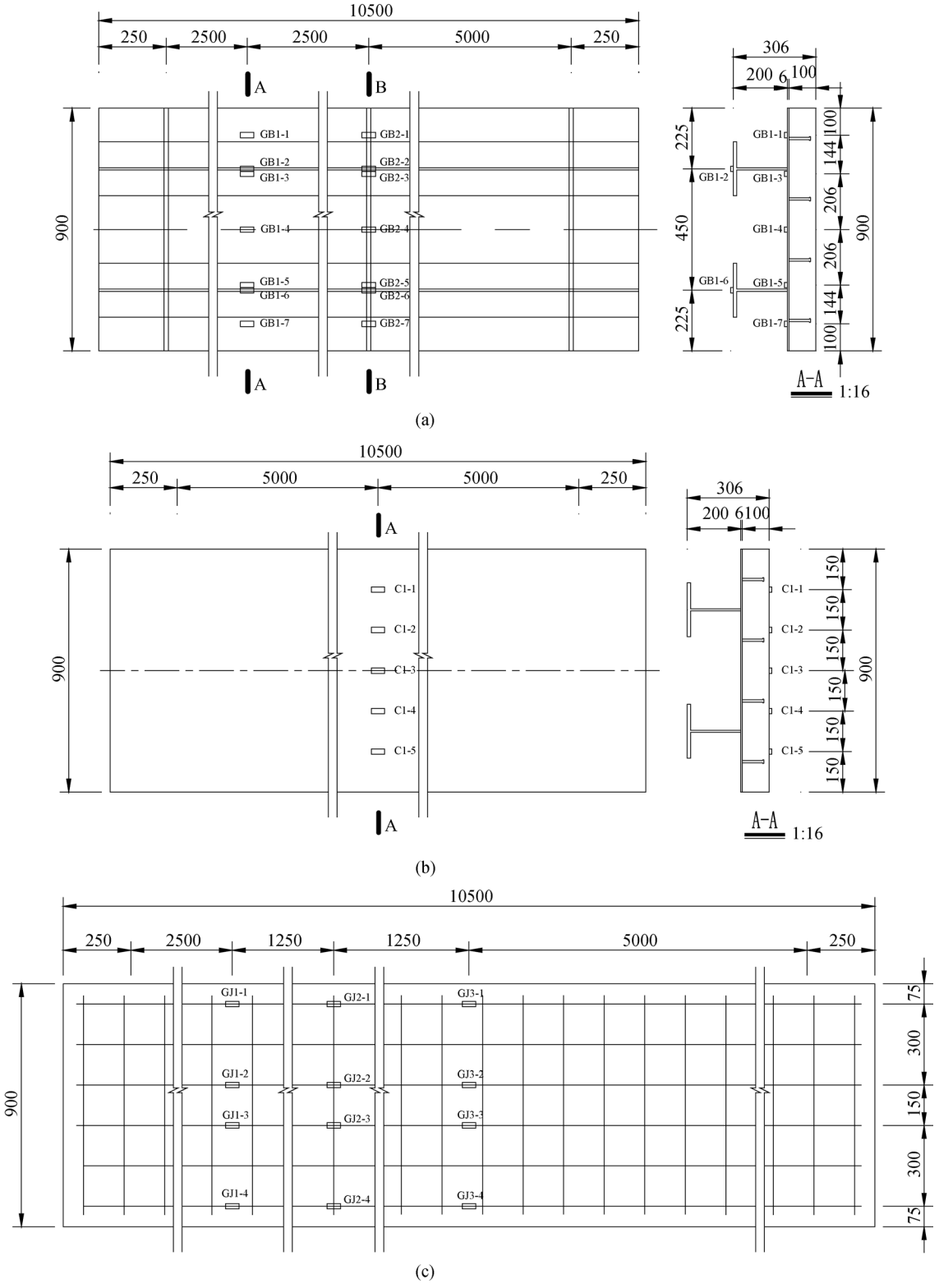

Fig. 3 Layout of strain gauges of the specimen S-1 and S-2. (a) Layout of longitudinal strain gauges of the steel plate; (b) layout of strain gauges in the concrete; (c) layout of strain gauges of steel bars

Table 1 Material properties of steel

name	diameter/thickness (mm)		yield strength (MPa)	tensile strength (MPa)
	design value	measured value		
steel bar	20	—	477.23	625.21
steel plate	6	5.67	377.83	543.64
steel plate	8	7.97	432.16	544.37
steel plate	9	8.99	398.64	535.72
steel plate	13	12.79	355.89	520.56
steel plate	14	13.9	375.05	539.25

the two specimens are then obtained as shown in Fig. 7. The ultimate load per meter of the two specimens was 903.7 kN and 865.9 kN, respectively. From the test results, it can be observed that the bearing capacity of this kind of composite bridge deck is higher than traditional OSDs or concrete plates according to the reported unit width ultimate load by other researchers [15–17].

3.4 Moment-curvature curve

The moment-curvature curve at section A and B (shown in Fig. 3(a)) of specimen S-1 and S-2 are drawn in Fig. 8. The moment-curvature curve could reflect the flexural rigidity of the specimen. As shown in Fig. 8, in sagging moment region (namely section A) specimen S-2 showed higher flexural rigidity than specimen S-1. While, in hogging moment region (namely section B), the flexural rigidity of the two specimens was similar.

Also, the moment-curvature curves of the specimens were converted to unit width moment-curvature curves by dividing the moment by the specimen width (0.9 and 1.1 for specimen S-1 and specimen S-2, respectively), as shown in Fig. 9. Same tendency with Fig. 8 was observed.

Table 2 Material properties of concrete (MPa)

cubic compressive strength	tensile strength	elasticity modulus
65.27	4.91	41556

Fig. 4 Failure mode of specimen S-1

Fig. 5 Failure mode of specimen S-2

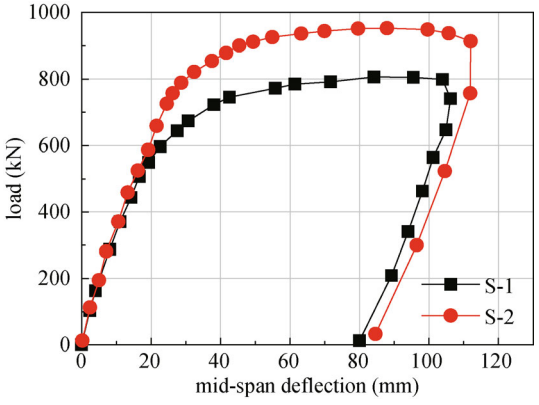

Fig. 6 Load versus mid-span deflection curves

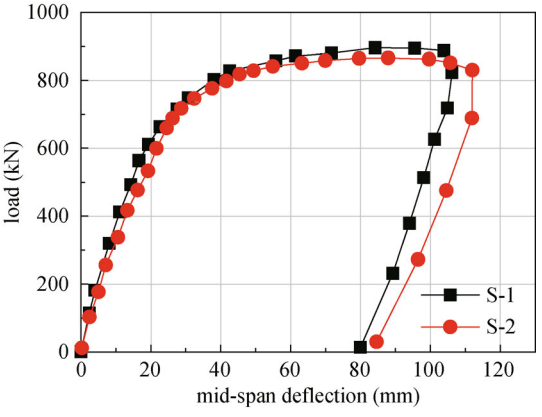

Fig. 7 Unit width load-deflection curves

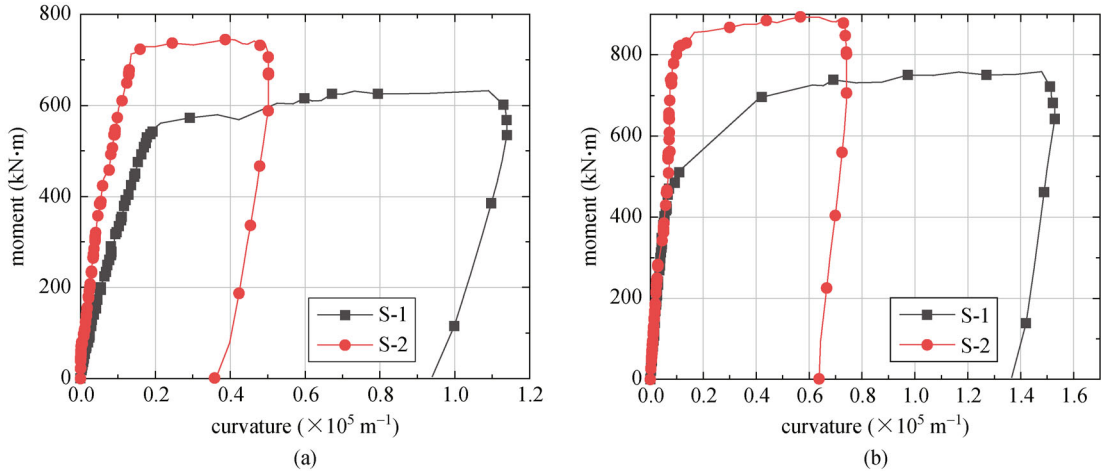

Fig. 8 Moment-curvature curve. (a) Section A; (b) section B

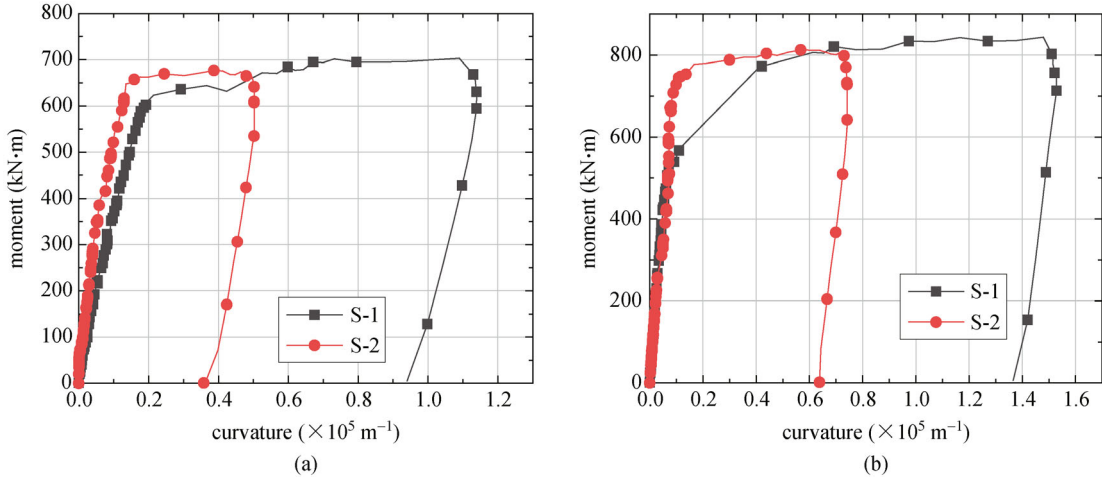

Fig. 9 Unit width moment-curvature curve. (a) Section A; (b) section B

3.5 Section bending capacity

The failure process of this kind of composite bridge deck can be concluded as: the yielding of bottom flange of T-shaped rib and cracking of concrete at section B-B, then followed the yielding of bottom flange of T-shaped rib and crushing of concrete at section A-A. Based on the knowledge described above and plastic design theory, the bending performance of composite bridge deck in positive and negative moment region was analyzed.

In negative moment region, because of the early cracking of concrete, concrete do not work at ultimate state, as shown in Fig. 10. The ultimate bending moment in negative moment region can be expressed by:

$$M_{un} = A_s f_s h_s + A_{p2} f_y h_{p2}, \quad (1)$$

where M_{un} = negative ultimate bending moment; A_s = cross-sectional area of rebar; f_s = yield strength of rebar; A_{p1} = area of compressive region of OSD section; A_{p2} = area of tensile region of OSD section; f_y = yield strength of steel plate.

In positive moment region, concrete and steel plate both contribute to the loading capacity at ultimate state as shown in Fig. 11. The ultimate bending moment in positive moment region can be expressed by:

$$M_{up} = bxf_{ck}h_c, \quad (2)$$

where M_{up} is positive ultimate bending moment; b is width

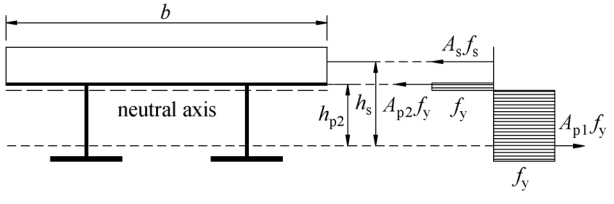

Fig. 10 Negative bending moment

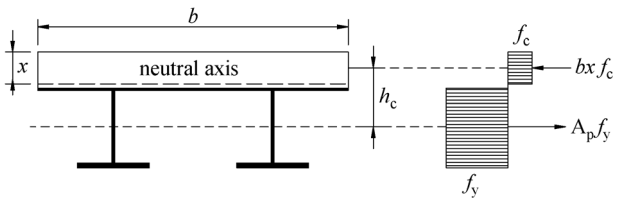

Fig. 11 Positive bending moment

of concrete plate; x is height of concrete compressive region; $f_{ck} = 0.64 f_{ck}$, f_c is cubic compressive strength. The coefficient 0.64 is used to convert cubic compressive strength to standard compressive strength according to the code [20].

The full width bending capacity of the two specimens in positive and negative moment region was calculated using Eqs. (1) and (2) and compared with tested results, as shown in Table 3. Calculated ultimate bending capacity of specimen S-1 showed good agreement with tested values, and the error was within 3%. However, the condition for specimen S-2 was not so optimistic, the error of ultimate negative moment reach 12.5%. This may be caused by two reasons: one reason is that a posit that full depth of the section enter plastic stage is adopted in theory calculation, while an elastic core may exist in the specimen; another reason attribute to the uncertainty of yield development during the experiment process.

4 Conclusions

Static loading test of two two-span continuous composite bridge decks specimens with T-shaped ribs was conducted, and the following conclusions can be drawn:

1) Under the concentrated load at mid-span sections, cracking of concrete and yielding of bottom flange of T-shaped rib at intermediate support section appeared first and then crushing of concrete and yielding of bottom flange of T-shaped rib at mid-span section followed.

2) The load-deflection curve showed that this kind of composite bridge deck exhibited good elastic and plastic performance. The ultimate bending capacities in positive and negative regions fit well with the calculated values.

3) The applied load on orthotropic composite bridge deck in this paper was far larger than the vehicle load stipulated in current specification. This kind of composite deck can better adapt to the overload condition of highway vehicles in China. Therefore, the orthotropic composite deck with T-shape ribs can be used in real bridges.

Acknowledgements This research was sponsored by Key Project of Chinese National Programs for Fundamental Research and Development (973 Program, No. 2013CB036303), the National Natural Science Foundation of China (Grant No. 51408424) and the Key Project of Jiangxi Province for Fundamental Research and Development (No. 20165ABC28001). These supports are gratefully acknowledged.

References

1. Yang Y D, Li T. The trend of the steel-concrete composite bridge in Japan. World Bridges, 1998, (4): 39–42
2. Wu C. Modern Steel Bridge. Beijing: China Communications Press, 2006
3. Muttoni A, Fernández Ruiz M. Concrete cracking in tension members and application to deck slabs of bridges. Journal of Bridge Engineering, 2007, 12(5): 646–653
4. Lachemi M, Hossain K M A, Ramcharitar M, Shehata M. Bridge deck rehabilitation practices in North America. Journal of Infrastructure Systems, 2007, 13(3): 225–234
5. Shiotani T, Ohtsu H, Momoki S, Chai H K, Onishi H, Kamada T. Damage evaluation for concrete bridge deck by means of stress wave techniques. Journal of Bridge Engineering, 2012, 17(6): 847–856
6. An Q H. Characteristic of stress in the joint between longitudinal U-rib and cross beam in orthotropic steel bridge deck. World Bridge, 2009(4): 26–29
7. Li Z X, Chan T H T, Ko J M. Fatigue damage model for bridge under traffic loading: Application made to Tsing Ma Bridge. Theoretical and Applied Fracture Mechanics, 2001, 35(1): 81–91
8. Battista R C, Pfeil M S, Carvalho E M L. Fatigue life estimates for a slender orthotropic steel deck. Journal of Constructional Steel Research, 2008, 64(1): 134–143
9. Huangi W, Lin G P, Qian Z D. Fracture-mechanics analysis of the fatigue life of the pavement on orthotropic steel bridge decks. China Civil Engineering Journal, 2006, 39(9): 112–116, 122 (in Chinese)
10. Chen J G. Preliminary study of design method of steel-concrete composite slab. Thesis for the Master's Degree. Chengdu: Southwest Jiaotong University, 2004 (in Chinese)
11. Mäkeläinen P, Sun Y. The longitudinal shear behaviour of a new steel sheeting profile for composite floor slabs. Journal of Constructional Steel Research, 1999, 49(2): 117–128
12. Marčiukaitis G, Jonaitis B, Valivonis J. Analysis of deflections of composite slabs with profiled sheeting up to the ultimate moment.

Table 3 Ultimate flexural capacity (kN·m)

specimens	positive moment			negative moment		
	calculated values	experimental values	error	calculated values	experimental values	error
S-1	763.2	742.4	2.8%	547.2	548.4	0.20%
S-2	919.5	847.5	8.5%	614.3	690.9	12.50%

Journal of Constructional Steel Research, 2006, 62(8): 820–830
13. Marimuthu V, Seetharaman S, Arul Jayachandran S, Chellappan A, Bandyopadhyay T K, Dutta D. Experimental studies on composite deck slabs to determine the shear-bond characteristic (m-k) values of the embossed profiled sheet. Journal of Constructional Steel Research, 2007, 63(6): 791–803
14. Seres N, Dunai L. Experimental and numerical studies on concrete encased embossments of steel strips under shear action for composite slabs with profiled steel decking. Steel and Composite Structures, 2011, 11(1): 39–58
15. Kim H Y, Jeong Y J. Experimental investigation on behaviour of steel-concrete composite bridge decks with perfobond ribs. Journal of Constructional Steel Research, 2006, 62(5): 463–471
16. Kim H Y, Jeong Y J. Steel-concrete composite bridge deck slab with profiled sheeting. Journal of Constructional Steel Research, 2009, 65(8–9): 1751–1762
17. Kim H Y, Jeong Y J. Ultimate strength of a steel-concrete composite bridge deck slab with profiled sheeting. Engineering Structures, 2010, 32(2): 534–546
18. Ren J. Experimental study on fatigue of composite steel-concrete structure. Thesis for the Master's Degree. Chengdu: Southwest Jiaotong University, 2006 (in Chinese)
19. China P R. Ministry of Communications. JTG D60–2015, General Code for Design of Highway Bridges and Culverts, 2015 (in Chinese)
20. China P R. Ministry of Housing and Urban-Rural Development. GB50010–2011, Code for design of concrete structures, 2011 (in Chinese)